International Journal of Solids and Structures 47 (2010) 2982–2990

Contents lists available at ScienceDirect

International Journal of Solids and Structures

journal homepage: www.elsevier.com/locate/ijsolstr

A micromechanical model for the Young's modulus of adipose tissue

Kerstyn Comley, Norman A. Fleck *

Department of Engineering, Cambridge University, Cambridge CB1 2PZ, UK

ARTICLE INFO

Article history:
Received 6 January 2010
Received in revised form 19 April 2010
Available online 6 August 2010

Keywords:
Adipose tissue
Foams
Micromechanics
Rheology

ABSTRACT

The microstructure of porcine adipose tissue is examined, and a micromechanical model is proposed for the dependence of overall effective modulus upon the moduli of the constituent microstructural units. Scanning electron microscopy and confocal microscopy reveal that the woven collagen network surrounding each adipocyte resembles a closed cell foam of relative density $\bar{\rho}_m = 0.1$, while the collagen interlobular septa behave as an open cell foam of relative density $\bar{\rho}_s = 3 \times 10^{-4}$. The measured viscosity of the lipid within the adipocytes is η = 36.8 mPa s at 37 °C; this is sufficiently small for the lipid to be idealised as an incompressible inviscid fluid. It is argued that the modulus of adipose tissue is dictated by the collagen network that surrounds the adipocytes. The volume fraction of the interlobular septa is sufficiently low that it provides a negligible contribution to the macroscopic modulus.

© 2010 Elsevier Ltd. All rights reserved.

1. Introduction

Subcutaneous adipose tissue is a soft connective tissue located directly beneath the dermis (Goldberg and Rabinovitch, 1983). It comprises collagen-based fibrous networks reminiscent of both open celled and closed cell foams. These multi-scale architectures endow the tissue with its finite stiffness, and the aim of the present study is to determine the relationship between microstructure and macroscopic modulus. The tissue fulfils a wide variety of multifunctional roles: it provides thermal insulation, allows for energy storage, and acts as a shock mitigator, yet it must possess a sufficiently low stiffness in order to allow for the free movement of underlying muscle groups. Prosthetic and drug delivery devices interact with the adipose layer in a manner which depends upon its stiffness, strength and toughness. For example, Shergold and Fleck (2004) have developed a mechanical model for skin penetration, and they show that the penetration force depends upon the Young's modulus and toughness of the tissue. In order to make predictions of the penetration force for adipose tissue, the first step is to measure its Young's modulus, and to develop a micromechanical model to relate its underlying microstructure to the macroscopic properties.

In the current study, a micromechanical model is developed to relate the microstructure of adipose tissue to its macroscopic modulus of elasticity. We begin by reviewing previous observations on the microstructure and mechanical properties of adipose tissue. Two experimental studies are reported: (i) observation of the microstructure of the extra-cellular matrix of porcine adipose tissue, based upon optical, confocal and scanning electron microscopy; and (ii) measurement of the viscosity of porcine lipid. It is found that the viscosity of lipid is sufficiently low for the lipid to behave as an incompressible inviscid fluid: its main mechanical role is to enforce incompressibility upon the overall response. A micromechanical model is then developed for the effective stiffness of the tissue, and is used to account for the Young's modulus as measured in a previous study (Comley and Fleck, 2009).

1.1. Review of the anatomy of adipose tissue

Adipose tissue largely comprises lipid-filled biological cells called *adipocytes*. Each adipocyte comprises a single lipid vacuole and a nucleus within a phospholipid bilayer (Shaw, 1901; Sheldon, 1965). In both human and porcine tissue the diameter of each adipocyte is fairly uniform at 80 μm (Bjorntorp and Martinsson, 1966; Mersmann et al., 1975). The biological cell membrane is a phospholipid, similar to that in other animal cells.

The adipocytes are supported externally by two collagen-based structures: a collagen mesh which surrounds each adipocyte (herein termed the *reinforced basement membrane*), and a predominantly type I collagen fibre network termed the *interlobular septa*, see Fig. 1, (Abrahamson, 1986; Brooks and Perosio, 1997). Additionally, but serving negligible mechanical function, are blood vessels, nerves and other structures such as follicles and cysts (Urmacher, 1997). The intervening space is filled with *ground substance*. 60–80 mass % of the adipose tissue is lipid, 5–30 mass % is water and the remaining 2–3 mass % is composed of proteins (Greenwood and Johnson, 1983).

The lipid is a light viscous oil of triacylglycerols (also known as triglycerides) whose molecular weight is on the order of 900 g/mol (Cormack, 1987). Triacylglycerols comprise fatty acids esterified to

* Corresponding author.
E-mail address: naf1@cam.ac.uk (N.A. Fleck).

0020-7683/$ - see front matter © 2010 Elsevier Ltd. All rights reserved.
doi:10.1016/j.ijsolstr.2010.07.001

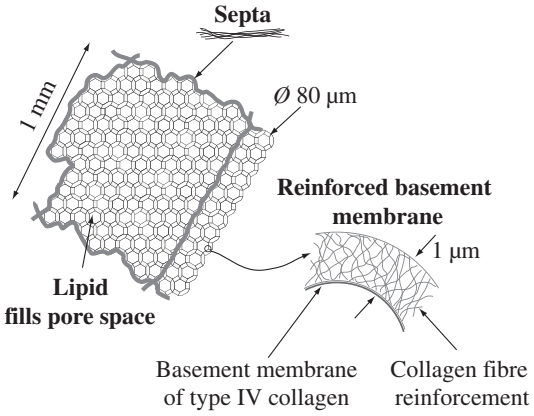

Fig. 1. A sketch of a lobule of adipose tissue.

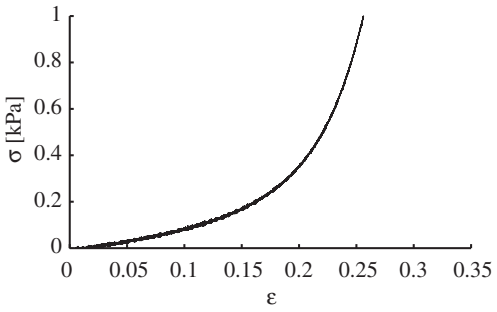

Fig. 2. Uniaxial compressive stress versus strain response of adipose tissue at $\dot{\varepsilon} = 0.002\ s^{-1}$ (taken from Comley and Fleck (2009)).

glycerol. Each fatty acid is a carboxylic acid with a long hydrocarbon tail (CH_2) in saturated or unsaturated form (Lodish et al., 2004; Snider et al., 2006). Porcine lipid has a higher proportion of stearic and oleic fatty acids and less palmitic acid than human tissue (Brockerhoff et al., 1966); despite this, the overall viscous properties are similar (Douglas, 1972).

Mature adipocytes are arranged within ill-defined lobules of diameter about 1 mm. Each adipocyte is in contact with at least one capillary (Greenwood and Johnson, 1983) and is entirely surrounded by reinforced basement membrane, a woven filamentous collagenous structure, see Fig. 1. This structure is loosely comprised of two distinct regions of collagen:

(i) a basement membrane (of thickness about 100 nm) of sheet-like type IV collagen adjacent to the phospholipid membrane of the adipocyte (Abrahamson, 1986), and
(ii) an outer sheath of fibrillar collagen (of thickness about 2 μm). Indirect immunofluorescence techniques have identified that the outer sheath contains a mixture of types I, III, V and VI collagen along with laminin, proteoglycans and other glycoproteins (Nakajima et al., 1998).

Threading through the lobules of adipocytes are long fibrous bundles of predominantly type I collagen known as the interlobular septa, as sketched in Fig. 1 (Urmacher, 1997). The septa bundles are several millimetres in length and can range in diameter from 10 nm (for a single fibre) to 30 μm (for a bundle of fibres). They share a similar structure to that of fibrous collagen bundles in the dermis. Arteries and veins align with the septa (Urmacher, 1997; Haake et al., 2001).

1.2. Review of the mechanical properties of adipose tissue

In uniaxial compression tests adipose tissue exhibits a non-linear stress versus strain response: at low strain levels, the response is linear whereas at strain level above 30%, the tissue 'locks-up' and the stress level increases rapidly. A representative stress versus strain curve at a strain rate of $\dot{\varepsilon} = 0.002\ s^{-1}$ is provided in Fig. 2. The tissue also shows a non-linear dependency upon strain rate. At low strain rates adipose tissue has a Young's modulus $E^* \approx 1$ kPa, whereas at strain rates of order $\dot{\varepsilon} = 1000\ s^{-1}$ the modulus increases by more than three orders of magnitude to $E^* \approx 3$ MPa (Miller-Young et al., 2002; Nightingale et al., 2003; Gefen and Haberman, 2007; Comley and Fleck, 2009).

Cyclic tests at low levels of strain amplitude ($<1 \times 10^{-3}$) reveal that adipose tissue behaves as a linear visco-elastic solid: at frequencies below 100 Hz the compressive storage modulus equals 2 kPa and the compressive loss modulus E'' equals 0.5 kPa (Patel et al., 2005; Schoemaker et al., 2006; Geerligs et al., 2008).

A number of previous studies on open and closed cell foams have sought to determine the relationship between the macroscopic properties of a foam and its microstructure (Huber and Gibson, 1988; Brocca et al., 2001; Gong et al., 2005; Sullivan et al., 2008). The use of foam models to represent the microstructure of animal and plant tissues has also been considered in a number of studies (Rajan, 1985; Budiansky and Kimmel, 1987; Georget et al., 2003). However, there remains a scientific challenge to relate the macroscopic elastic response of adipose tissue to the elastic properties of its underlying microstructure. This is hampered by the fact that the Young's moduli for the septa and for the reinforced basement membrane are not known, to the authors' knowledge. Herein, we shall assume that the collagen fibres that make up the interlobular septa have a similar modulus to that of collagen bundles in tendons, $E_S \approx 1$ GPa (Benedict et al., 1968; Sanjeevi et al., 1982; Haut, 1983). However, a wide range of values are reported in the literature for the basement membrane in other types of tissue. For example, Candiello et al. (2007) found that the retinal basement membrane, of thickness 402 nm, and comprising woven type IV collagen, has a modulus of $E_m = 3$ MPa. Codd et al. (1994) found that the ovine basement membrane of the tracheal wall, of thickness of 50 μm and again comprising type IV collagen, has a Young's modulus of approximately $E_m = 20$ kPa. These major differences in modulus are consistent with the fact that the tissues serve very different mechanical functions, and may be attributed to differences in morphology of microstructure such as the degree of waviness of the fibres. In the present study we infer the properties of the reinforced basement membrane from the known stiffness of adipose tissue.

2. Experimental method

2.1. Investigation of the microstructure

Rectangular blocks of freshly harvested porcine adipose tissue have been cut to a depth of 3–10 mm below the dermis. The arrangement of the reinforced basement membrane and the interlobular septa is studied, including the effect of uniaxial tension and compression upon the deformed microstructure. The microstructural results presented here are for a single pig, but additional observations were performed on samples from a further five pigs. The results from the single pig were found to be representative of the results from all the pigs and therefore, for brevity the additional results are considered no further in the present study.

2.1.1. Observation of the reinforced basement membrane

The microstructure of the reinforced basement membrane has been explored using a scanning electron microscope (FEI Philips

XL30 FEGSEM), and a laser confocal microscope (Leica DM IRBE, 488 nm laser line, 590–700 nm scan spectrum). Specimens of dimension 10 mm by 3 mm by 5 mm were fixed, and the lipid and phospholipid cell membranes were removed by chemical action. Six samples were prepared for viewing by a scanning electron microscope (SEM) and two samples were prepared for viewing with a confocal microscope. The details on sample preparation are given in Appendix A. Measurements of the dimensions of the reinforced basement membrane were taken from 40 cells, randomly chosen from eight sections (four sections from each sample) obtained via the confocal microscope using 20x and 63x water immersion objectives. The thickness of each section was approximately 2 μm. The standard point counting method was used to estimate of the volume fraction of the collagen network from fifty randomly selected confocal microscope sections (25 sections from each specimen), using a 20x objective (Myking, 1988; Reith and Mayhew, 1988). In each case examination of plots of cumulative mean and variance indicated adequate sampling of the specimens.

2.1.2. Observation of the interlobular septa

SEM and light microscopy have been used to observe the microstructure of the interlobular septa. The SEM specimens described above were re-used and three additional histological sections of adipose tissue of dimension 4 μm by 5 mm were prepared for viewing by light microscopy. During preparation of the histological sections the tissue was stained with hematoxylin and counterstained with eosin (H & E stains collagen red); full details of the preparation methods are given in Appendix A.

2.1.3. Observation of the deformed microstructure

Three freshly harvested specimens of adipose tissue, of dimension width $W = 10$ mm, length $L = 25$ mm and thickness $B = 10$ mm, were subjected to tensile strain of 6% or a compressive strain of 15%, and were then fixed and observed using the confocal microscope. After applying the tensile strain, the ends of the specimen were fastened to a glass slide with a cotton thread binding. In the compression tests, the specimen was compressed between two PMMA blocks (15 mm by 15 mm by 5 mm). The blocks and specimen were then fastened to a glass slide with cotton thread binding to prevent unloading of the tissue. Additionally, a control specimen was not subjected to an applied strain.

The strain levels in the tension and compression tests were of sufficient magnitude to deform the extra-cellular matrix by a discernable amount, without risking rupture of the adipocytes or generating tissue lock-up (see Fig. 2). After deformation, the specimens were chemically processed for viewing with a confocal microscope according to the procedure described in Appendix A: the tissue was fixed and the lipid was removed. After fixing of the specimens, the clamping and glass slides were removed and the specimens were trimmed to 3 mm thick (by removal of tissue from the top and bottom faces) to improve the quality of the micrographs. Six microscope sections were taken from different locations on each specimen. Additional observations were performed on specimens that had been fixed but without chemical removal of the lipid; these confirmed that removal of the lipid did not alter the morphology of the deformed collagen network.

2.2. Visco-elastic tests on the lipid

Calibration of the micromechanical model requires measurements to be made of the shear properties of the lipid contained within the adipocytes. A series of rheological experiments have been performed in order to measure the complex shear modulus of the lipid as a function of frequency.

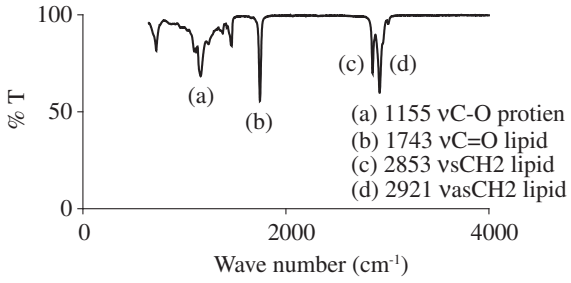

Fig. 3. Fourier transform infrared spectroscopy (FTIR) characterisation of lipid extracted from porcine adipose tissue.

2.2.1. Sample preparation

Lipid was extracted from adipose tissue by squeezing the tissue between loading platens, as follows. Fresh porcine tissue, of rectilinear dimension $20 \times 30 \times 5$ mm, was wrapped in rip-stop nylon and compressed, under dry conditions, between platens at a constant load of 9.5 kN and at 40 °C for at least 10 min. All equipment was sterilized before use to limit the breakdown of the lipid by enzymes. The liquid recovered by filtration through the rip-stop nylon was centrifuged at 4000 rpm for 10 min resulting in a top layer of light viscous oil, and this top layer has been identified by Angel and Sheldon (1965) as the lipid content. Two denser layers were also separated from the recovered liquid: an opaque highly viscous layer of cell debris, and an aqueous-based phase containing blood and lymph. The lipid layer was removed for testing.

The composition of the extracted liquid was confirmed with Fourier transform infrared spectroscopy (FTIR) (see Fig. 3). Peaks were found at frequencies 1743, 2853 and 2921 cm^{-1}, all of which are characteristic peaks for lipid (Maziak et al., 2007). A smaller peak was also observed at 1155 cm^{-1}, characteristic of υC-O side chain groups in proteins. These results suggest that the extracted liquid was predominantly lipid with negligible contamination by collagen proteins.

2.2.2. Experimental procedure

The oscillatory shear response of the lipid was measured as a function of frequency over the range 0.1 Hz–8 kHz by two types of parallel plate rheometer, as follows.

(i) At frequencies in the range 0.1–16 Hz an ARES rotational rheometer[1] was used and operated in a strain-controlled mode, with a pair of parallel plates of diameter 25 mm and spacing of 0.75 mm. These tests were performed both at 25 °C and at 37 °C. See Barnes et al. (1993) for details on the operation of this type of rheometer.

(ii) At higher frequencies, in the range 10 Hz–8 kHz, a piezoelectric axial vibrator (PAV) squeeze-flow rheometer was used. The PAV comprises a pair of vibrating stainless steel plates of separation 61 μm; the liquid sample is in the form of a cylindrical droplet of diameter 20 mm and height 61 μm, and is held in place by surface tension. Tests were only performed at 25 °C, due to limitations of the test equipment. A piezoelectric drive squeezes the liquid specimen in an oscillatory manner, and piezoelectric sensors measure the harmonic force as a function of shear strain γ. A full description of the device and the data reduction method are given by Crassous et al. (2005).

Both rheometers performed 'frequency sweeps' in which the frequency was incrementally increased with a fixed shear strain

[1] Advanced Rheometric Expansion System, TA Instruments, USA.

amplitude of 10^{-2} for the rotational rheometer, and 10^{-5} for the squeeze-flow rheometer. Preliminary tests over a range of strain amplitudes were used to confirm that the lipid behaves in a *linear* visco-elastic manner.

3. Results

3.1. Dimensions of the reinforced basement membrane

The SEM investigation reveals that the basement membrane has an outer sheath of fibrillar collagen, see Fig. 4. This supports previous observations by Nakajima et al. (1998). The fibrillar collagen resembles a closed cell foam in morphology, see the image in Fig. 5a from confocal microscopy. An average diameter $d = 77 \pm 17$ μm (±1 s.d.) and wall thickness $h = 1.9 \pm 0.4$ μm (±1 s.d.) were measured from 40 cells, using the confocal microscope. (In each measurement, the depth of the z-axis was adjusted to that of the centre plane of each cell). This value of cell diameter is comparable to that measured for porcine and human adipocytes, as reported by Bjorntorp and Martinsson (1966) and Mersmann et al. (1975). Confocal micrographs of the type shown in Fig. 5a were also used to measure a volume fraction $\bar{\rho} = 0.17 \pm 0.02$ (±1 s.d.) of collagen in the reinforced basement membrane and the septa fibres.

3.2. Morphology of the septa

The fibrous nature of the individual septa bundles has been observed using SEM, see Fig. 6a. Light microscopy on a histological section proved to be a more suitable technique for revealing the degree of connectivity of the septa fibres. A typical image is given in Fig. 6b. The septa bundles form a 3D network resembling that of an open cell foam with a cell edge length, $l = 1$ mm and a cell wall thickness of $h = 10$ μm. The volume fraction of septa fibres is estimated by using the formula for an open cell foam of cubic arrangement: the volume fraction is $\bar{\rho} = 3h^2/l^2 = 3 \times 10^{-4}$. We note in passing that the morphology of the septa fibres resembles that of polymeric and metallic foams, see for example Jang et al. (2008).

3.3. Measurements of the deformed collagen network under uniaxial loading

Inspection of confocal images of the collagen network in the as-received and deformed configurations (Fig. 5) reveals that the integrity of the foam structure is maintained with no evidence of relative rotation or rearrangement of neighbouring cells. The cross-section of the cells stretches from a circular to an elliptical shape. Under tension the long axis aligns with the loading axis, whereas under compression the long axis is transverse to the direction of compressive straining.

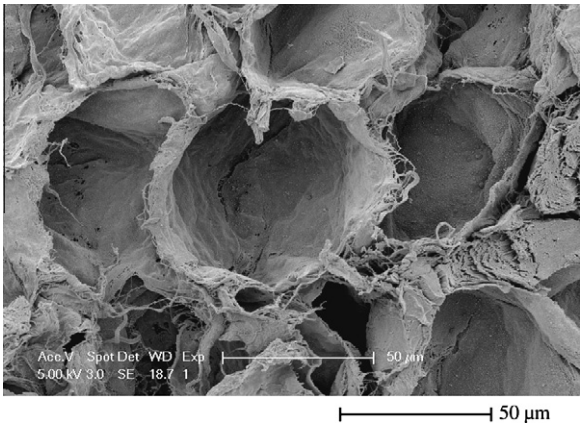

Fig. 4. Scanning electron micrograph of porcine type IV collagen basement membrane, reinforced with collagen fibrils.

A check was made to assess whether the local straining of the cells matched the macroscopic applied strain in order to confirm that affine deformation occurs. Measurements were taken of the major and minor diameters of five cells randomly selected from each microscope section. Six sections were examined from different locations on each specimen (giving a total of 30 measurements for each specimen). At low levels of applied strain it is assumed that the maximum cross-sectional area of the cell remains constant. Therefore, the diameter of the cell, in a relaxed state, could be estimated from the dimensions of the deformed cell, and subsequently the level of strain in the direction of the principle axis could be measured. An average tensile strain of 7% ± 6% (±1 s.d.) was observed in cells under a macroscopic tensile strain of 6% and an average compressive strain of 23% ± 6% (±1 s.d.) was observed in cells under a macroscopic compressive strain of 20%. We deduce that the extra-cellular matrix deforms in an affine manner, with negligible rearrangement of neighbouring cells.

3.4. Visco-elastic properties of the lipid

The visco-elastic measurements revealed that the lipid behaves as a linear viscous fluid with a viscosity of $\eta = 60.6 \pm 2$ mPa s (±1 s.d.) at 25 °C. The viscosity drops to $\eta = 36.8 \pm 1$ mPa s (±1 s.d.) at 37 °C, see Fig. 7. The storage shear modulus was on the order of $G_l = 0.01$ Pa which is comparable to the resolution of the rheometers. Thus, the elastic shear modulus of the lipid is much less than that of adipose tissue (as reported above in the introduction), and can be neglected.

4. Discussion

4.1. A micromechanical model for the effective modulus of adipose tissue

A micromechanical model is now proposed to account for the magnitude of Young's modulus $E^* = 1$ kPa for adipose tissue at low strain rates. The adipose tissue is idealised as a closed cell foam of reinforced basement membrane ($\bar{\rho}_m = 0.1$), along with an interpenetrating network of septa fibres with low volume fraction, $\bar{\rho}_s = 3 \times 10^{-4}$ (see Fig. 8). The basement membrane is filled with lipid of volume fraction $\bar{\rho}_l = 1 - \bar{\rho}_m - \bar{\rho}_s \approx 0.9$. The measured viscosity of the lipid is sufficiently low for it to behave as an incompressible inviscid fluid.

We proceed to establish a Voigt upper-bound for the overall effective Young's modulus by summing together the contributions from the reinforced basement membrane and septa fibres. Write the Young's modulus of the basement membrane and septa fibres as E_m and E_s, respectively. Gibson and Ashby (1997) argue that the contribution to overall modulus from a closed cell foam of cell wall modulus E_m and volume fraction $\bar{\rho}_m$ is $\bar{\rho}_m E_m$, see their Eq. (5.13). This coincides with the result for a Voigt upper-bound. Upon writing E_s^* as the contribution to effective modulus from the septa fibres, the overall modulus of adipose tissue E^* is

$$E^* = \bar{\rho}_m E_m + E_s^*. \tag{1}$$

It remains to compare the relative magnitude of these two contributions.

4.2. Contribution of the interlobular septa network

An assessment is now made of the contribution of the septa network to the overall stiffness of the tissue. The micrographs

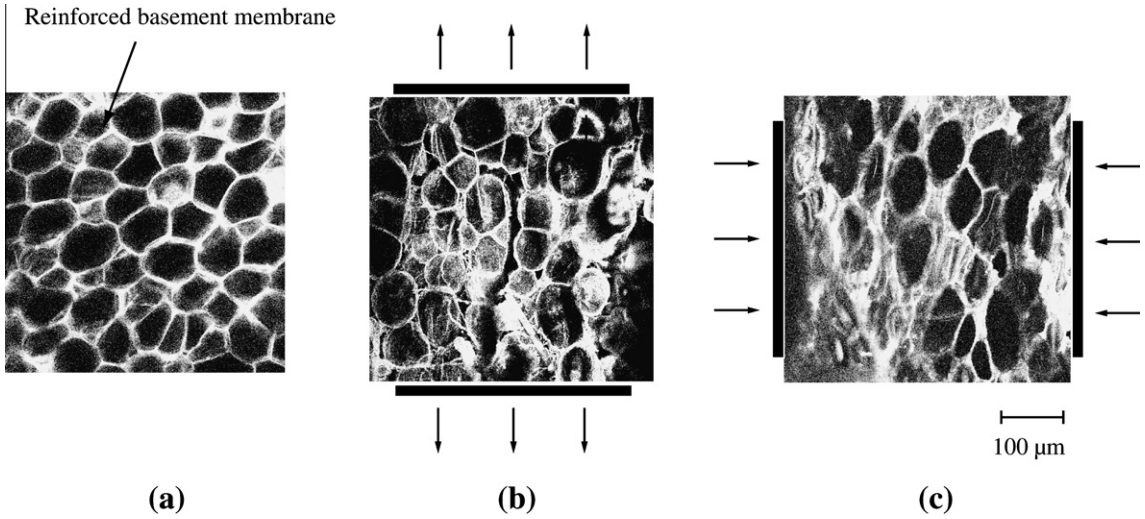

Fig. 5. Confocal microscope images of the deformed network of reinforced basement membrane, in (a) as-received; (b) uniaxial tension, $\varepsilon = 6\%$; (c) uniaxial compression, $\varepsilon = -20\%$.

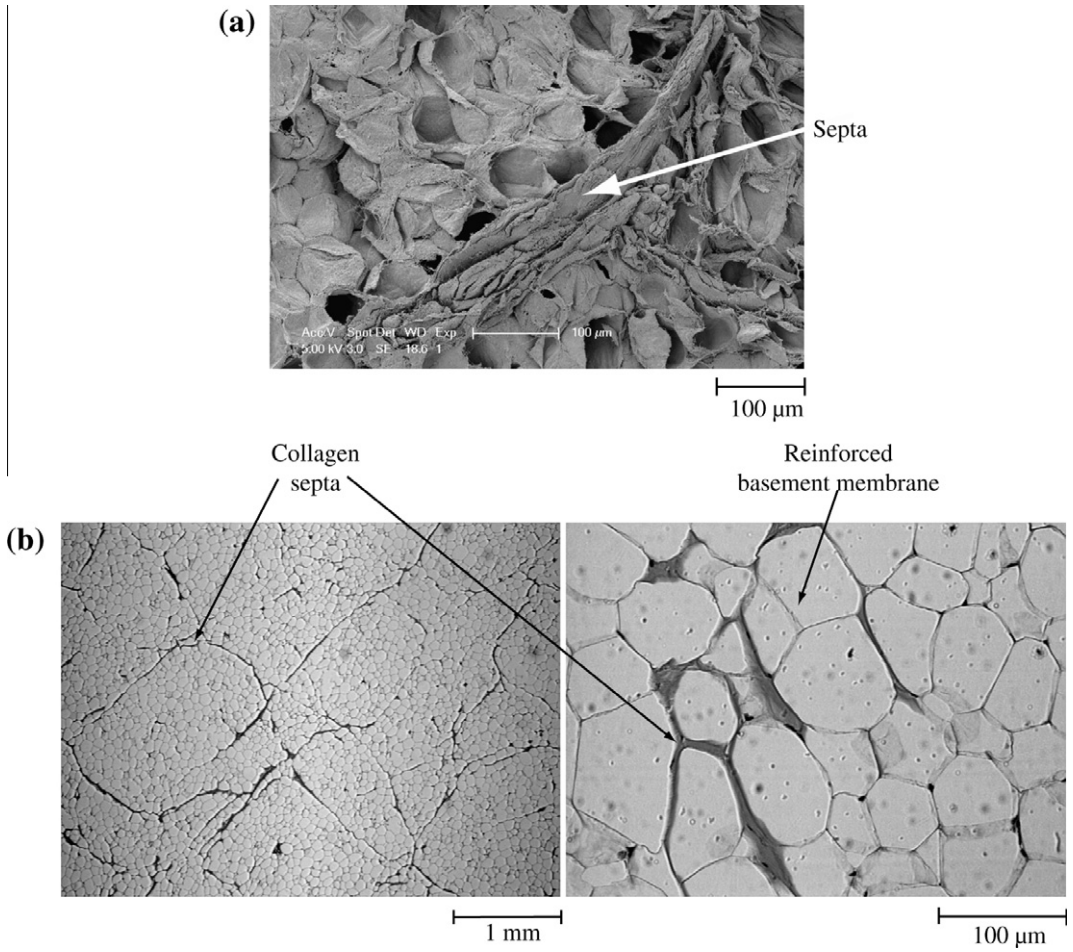

Fig. 6. (a) Scanning electron micrograph of septa surrounded by reinforced basement membrane. (b) Histological section of porcine adipose tissue at two magnifications showing septa and reinforced basement membrane. The collagen has been stained with hematoxylin and eosin (H & E).

of adipose tissue reported above indicate that the septa fibre network can be represented either by an open cell foam or by a meshwork of long wavy fibres, recall Fig. 6. Each of these two representations is now considered in order to obtain their contribution to the macroscopic modulus of the adipose tissue.

4.2.1. Septa represented as an open cell foam

The Young's modulus of an individual septa fibre is taken to equal that of a collagen fibre in a tendon, $E_s = 1$ GPa (Haut, 1983). Now the Young's modulus of an open cell foam E_s^* with struts made from a solid of modulus E_s and volume fraction is $\bar{\rho}_s$ (Gibson and Ashby, 1997)

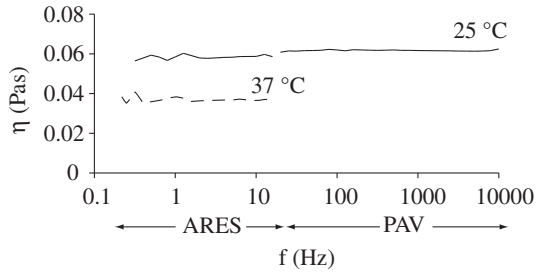

Fig. 7. Viscous response of lipid extracted from porcine adipose tissue at 25 °C (solid line) and 37 °C (dashed line). Tests were conducted at a strain of less than 1% over a frequency range of 0.015 Hz–8 kHz.

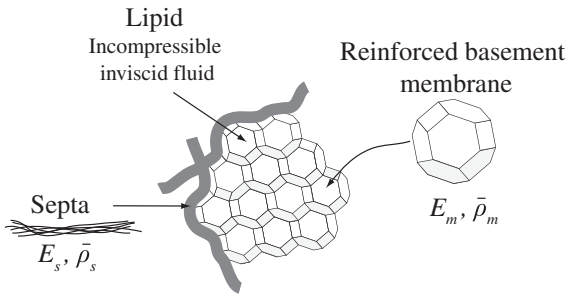

Fig. 8. A micromechanical model of adipose tissue comprising a lipid-filled closed cell foam of reinforced basement membrane and an open cell foam of septa fibres.

$$E_s^* \approx \bar{\rho}_s^2 E_s. \tag{2}$$

Upon substituting for $\bar{\rho}_s = 3 \times 10^{-4}$, we obtain $E_s^* = 90$ Pa; this contribution is minor in comparison with the overall value of $E^* = 1$ kPa for adipose tissue. The value of $E_s^* = 90$ Pa is likely to be an over-estimate, as the value $E_s = 1$ GPa is based on the relatively straight tendon fibres rather that wavy septa fibres.

4.2.2. Septa represented by a long fibre network

Consider, instead, a random isotropic distribution of long wavy fibres. Suppose the fibres occupy a volume fraction $\bar{\rho}_s$, and are made from a solid of Young's modulus E_s. Assume that the fibres have a circular cross-section of radius a_f, a sinusoidal waviness of amplitude w_0 and wavelength λ. The axial stiffness per unit length of the a fibre is given by

$$k = \frac{\pi a_f^4 E_s}{2 w_0^2}. \tag{3}$$

Now assume that the fibres are randomly orientated in space. Then, a virtual work calculation can be performed to obtain the Young's modulus of the solid as

$$E_s^* = \frac{\bar{\rho}_s k}{3\pi a_f^2} = \frac{1}{6}\bar{\rho}_s E_s \left(\frac{a_f}{w_0}\right)^2. \tag{4}$$

Now substitute values: $E_s = 1$ GPa, $\bar{\rho}_s = 3 \times 10^{-4}$ and $w_0 = 40a$, giving an overall modulus of the septa network $E_s^* = 31$ Pa. Note that the value of E_s^* is sensitive to the assumed level of waviness. An exact measure of the level of waviness of the septa fibres in adipose tissue is not available. However, examination of histology images (Fig. 6b) indicates that the septa have a high degree of waviness (on the order of $w_0 > 40a$). We again conclude that the contribution from the septa fibres to macroscopic modulus is minor and the dominant term on the right hand side of Eq. (1) is from the elastic response of the reinforced basement membrane.

4.3. Prediction of the modulus of the reinforced basement membrane

The structure of the reinforced basement membrane, as observed by microscopy (Figs. 4 and 5a), resembles a closed cell foam, as already noted in Section 3.1. An estimate for the effective modulus of a closed cell foam of volume fraction $\bar{\rho}_m$ and cell wall modulus E_m is

$$E^* = \bar{\rho}_m E_m, \tag{5}$$

upon specialising Eq. (1). Given a closed cell foam with $\bar{\rho}_m = 0.1$ (matching the measured volume fraction of reinforced basement membrane) and a Young's modulus of $E^* = 1$ kPa (matching the overall modulus of the tissue) the Young's modulus of the collagen network of the reinforced basement membrane is thereby estimated to be $E_m = 10$ kPa. This result is consistent with measurements of ovine tracheal wall membrane made by Codd et al. (1994).

It remains to consider in more detail the contribution to effective modulus from the reinforced basement membrane. The formula (5) neglects any contribution from the lipid inside the adipocytes. In reality, the lipid imposes a volumetric constraint upon the overall deformation and it possesses a finite bulk modulus. This leads to some modification of (5) and this is addressed as follows.

4.4. The elastic response of a fluid-filled closed cell foam

Recall that the lipid contained within the adipocytes behaves as an inviscid incompressible fluid. What is the influence of this fluid upon the macroscopic elastic properties of the closed cell foam? In order to explore this, we consider the idealised problem of a periodic cubic array of cells, each of side length l and wall thickness h, as shown in Fig. 9 ($l = 80$ μm and $h = 2$ μm, corresponding respectively to the cell diameter and cell wall thickness of the reinforced basement membrane). Previous studies have shown that a cubic cellular array provides a suitable, simplified representation of a closed cell foam structure of a soft tissue (Fung, 1975; Vawter et al., 1979; Rajan, 1985). The volume fraction follows immediately as $\bar{\rho} = h/l$. Each cell is filled with an inviscid fluid of bulk modulus K and pressure p. The cell walls are elastic plates made from an isotropic solid of in-plane Young's modulus E_m and Poisson ratio ν.

The stresses σ_{ij} within the cell wall are in equilibrium with the fluid pressure p, and the macroscopic applied stress state $(\Sigma_{11}, \Sigma_{22}, \Sigma_{33})$ is aligned with the material axes x_1, x_2, x_3 as shown in the Fig. 9. Denote the walls A, B and C using a superscript notation. Then equilibrium dictates that

$$\left(p + \sum_{11}\right)\ell^2 = h\ell\left(\sigma_{11}^B + \sigma_{11}^C\right), \tag{6a}$$

$$\left(p + \sum_{22}\right)\ell^2 = h\ell\left(\sigma_{22}^A + \sigma_{22}^C\right), \tag{6b}$$

$$\left(p + \sum_{33}\right)\ell^2 = h\ell\left(\sigma_{33}^A + \sigma_{33}^C\right), \tag{6c}$$

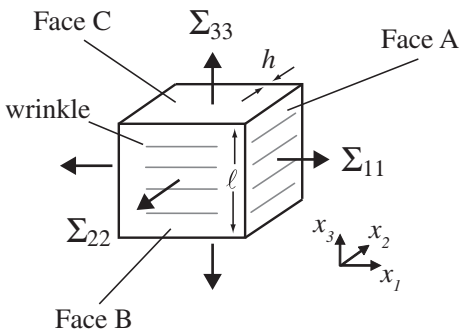

Fig. 9. A fluid-filled closed cell foam of cubic geometry.

as discussed previously by Warner et al. (2000). Assume that the wall stresses are related to the macroscopic strain state ε_{11}, ε_{22}, ε_{33} by the usual isotropic elasticity relations, for example

$$E_m\varepsilon_{33} = \sigma^A_{33} - \nu\sigma^A_{22} = \sigma^B_{33} - \nu\sigma^B_{11}. \tag{7}$$

Rearrangement of the above relations gives

$$\frac{2E_m}{1-\nu}\frac{h}{\ell}\begin{pmatrix}\varepsilon_{11}\\ \varepsilon_{22}\\ \varepsilon_{33}\end{pmatrix} = p\begin{pmatrix}1\\1\\1\end{pmatrix} + \frac{1}{\nu-2}\begin{bmatrix}-(\nu+2) & \nu & \nu\\ \nu & -(\nu+2) & \nu\\ \nu & \nu & -(\nu+2)\end{bmatrix}\begin{pmatrix}\Sigma_{11}\\ \Sigma_{22}\\ \Sigma_{33}\end{pmatrix}. \tag{8}$$

This is the general response of the fluid-filled foam under any combination of internal pressure p and external loading $(\Sigma_{11}, \Sigma_{22}, \Sigma_{33})$. It gives the contributions to wall stretch of the foam cell walls from the internal pressure and from the external stress state. We now use Eq. (8) in order to determine the effect of the pressurised fluid upon the macroscopic stiffness of the foam, first for hydrostatic loading and then for uniaxial loading. Then, we modify the relation for the case where wrinkles develop in faces A and B under external compressive loading $\Sigma_{33} \ll -p$.

4.4.1. The hydrostatic case

(i) Absent the fluid (i.e. $p = 0$), the closed cell foam dilates by a volumetric strain ε_H under an external hydrostatic loading of type $\Sigma_{11} = \Sigma_{22} = \Sigma_{33} = \Sigma_H$, and Eq. (8) reduces to $\varepsilon_H = \frac{\Sigma_H}{K^*}$ where

$$K^* = \frac{2}{3}\frac{E_m}{1-\nu}\frac{h}{\ell}. \tag{9}$$

K^* denotes the bulk modulus of the dry, closed cell foam.

(ii) Now suppose that the closed cell foam is first pressurised to a level p_0 and is then subjected to the additional external hydrostatic tension Σ_H. Under the internal pressure of p_0 alone, the foam acquires a volumetric strain of

$$\varepsilon_{H^0} = \frac{p_0}{K^*}. \tag{10}$$

Now apply the additional loading Σ_H, with the mass of the fluid held fixed. The fluid undergoes a change in volume due to a change in pressure according to

$$p - p_0 = -K(\varepsilon_H - \varepsilon_{H0}), \tag{11}$$

due to its finite compressibility K. Substitution of Eqs. (10) and (11) into Eq. (8) gives

$$\varepsilon_H = \varepsilon_{H0} + \frac{\Sigma_H}{K+K^*}. \tag{12}$$

We conclude that the presence of the fluid increases the effective bulk modulus of the foam from K^* to $K + K^*$.

4.4.2. The uniaxial response

Absent the fluid (i.e. $p = 0$), the closed cell foam responds to a uniaxial tensile stress Σ_{33} by a strain of magnitude

$$\varepsilon_{33} = \frac{2+\nu}{2-\nu}\frac{\Sigma_{33}}{3K^*}, \tag{13}$$

directly from Eq. (8).

Alternatively, the closed cell foam is first pressurised to a level p_0 and is then subjected to the additional uniaxial tension Σ_{33}. The constitutive law (8) and Eq. (11) then give

$$\varepsilon_{33} = \frac{p_0}{3K^*} + \left(\frac{2+\nu}{2-\nu} - \frac{K}{3(K+K^*)}\right)\frac{\Sigma_{33}}{3K^*}. \tag{14}$$

Consequently, the presence of the fluid reduces the uniaxial tangent compliance $C = d\varepsilon_{33}/d\Sigma_{33}$ from

$$C = \frac{2+\nu}{2-\nu}\frac{1}{3K^*}, \tag{15a}$$

to

$$C = \left(\frac{2+\nu}{2-\nu} - \frac{K}{3(K+K^*)}\right)\frac{1}{3K^*}. \tag{15b}$$

In order to assess the significance of this drop in compliance, consider the practical case where the fluid has a much higher bulk modulus K than that of the closed cell foam, K^*, and for simplicity take $\nu = 0$ for the cell wall material. Then, the presence of the fluid causes C to drop by one third from $1/(3K^*)$ to the value of $2/(9K^*) = 1/(\overline{\rho}E_m)$. We conclude that the presence of the fluid has a minor effect upon the uniaxial modulus.

4.4.3. The role of elastic buckling of the cell walls

The above analysis assumes that the cell walls remain in tension. However, in uniaxial compression of the fluid-filled closed cell foam such that $\Sigma_{33} \ll -p$, the stress components σ^A_{33} and σ^B_{33} become compressive and the cell walls A and B will wrinkle. First, we determine the critical value of Σ_{33} that causes the side faces of the unit cell to wrinkle. Then, the uniaxial tangent compliance is determined assuming that the side faces are in the wrinkled state.

The foam is first pressurised to a level p_0 and is then subjected to the additional uniaxial tension Σ_{33}, giving the uniaxial response equation (14). For small values of Σ_{33}, the stress components $\sigma^A_{33} = \sigma^B_{33}$ remain tensile and of magnitude

$$\sigma^A_{33} = \frac{E_m}{1-\nu^2}\varepsilon_{33} + \frac{\nu E_m}{1-\nu^2}\varepsilon_{22}, \tag{16}$$

via the elasticity relations for the cell walls of the type Eq. (7). Substitution of Eq. (8) into Eq. (16) gives

$$\frac{9K^*(1-\nu)}{E_m}\sigma^A_{33} = 3p_0 + \frac{2K+3K^*}{K+K^*}\Sigma_{33}. \tag{17}$$

Assume that the cell walls are sufficiently slender $(h/\ell \ll 1)$ such that the wrinkling stress is $\sigma^A_{33} = 0$. Substitution of this criterion into (17) gives

$$\Sigma_{33} = -\frac{K+K^*}{2K+3K^*}3p_0. \tag{18}$$

4.4.4. Post-wrinkling regime

Continue to load the fluid-filled foam with a more negative value of axial stress Σ_{33} than the critical value of Eq. (18). The faces A and B remain wrinkled such that $\sigma^A_{33} = \sigma^B_{33} = 0$. The equilibrium statement (6c) gives immediately that $p = -\Sigma_{33}$. Horizontal wrinkling of faces A and B leads to modified elasticity relations of

$$\sigma^A_{22} = \frac{E_m}{1-\nu^2}\varepsilon_{22} \quad \text{and} \quad \sigma^B_{11} = \frac{E_m}{1-\nu^2}\varepsilon_{11}, \tag{19}$$

and consequently Eq. (8) is modified to

$$\frac{E_m}{1-\nu^2}\frac{h}{\ell}\begin{pmatrix}\varepsilon_{11}\\ \varepsilon_{22}\end{pmatrix} = \frac{p}{2+\nu}\begin{pmatrix}1\\1\end{pmatrix} + \frac{1}{4-\nu^2}\begin{bmatrix}2 & -\nu\\ -\nu & 2\end{bmatrix}\begin{pmatrix}\Sigma_{11}\\ \Sigma_{22}\end{pmatrix}. \tag{20}$$

The axial strain ε_{33} follows from the constitutive law (11) for the fluid and from Eq. (20) to give

$$\varepsilon_{33} = \frac{(K+K^*)}{KK^*}p_0 + \frac{\Sigma_{33}}{K} + \frac{(1-\nu^2)}{(2+\nu)}\frac{\ell}{hE_m}(2\Sigma_{33} - \Sigma_{11} - \Sigma_{22}). \tag{21}$$

For the uniaxial case, $\Sigma_{11} = \Sigma_{22} = 0$, and the uniaxial tangent compliance follows as

$$C = \frac{d\varepsilon_{33}}{d\Sigma_{33}} = \frac{1}{k} + \frac{4}{3}\frac{(1+\nu)}{(2+\nu)}\frac{1}{K^*}. \quad (22)$$

Again, consider the practical case where the fluid has a much higher bulk modulus K than that of the closed cell foam, K^*, and for simplicity take $\nu = 0$ for the cell wall material. Then, the compliance C follows as $C = 2/(3K^*)$. Upon recalling that the uniaxial tangent compliance is $C = 2/(9k^*)$ for the case of a fluid-filled foam with unbuckled cell walls, we conclude that cell wall buckling leads to a drop in tangent stiffness by a factor of three. Also note that the empty foam with unbuckled cell walls has an uniaxial tangent compliance of $C = 1/(3K^*)$ according to (13). Thus, fluid-filling of the cell walls and cell-wall buckling lead to changes in macroscopic stiffness by a factor of about three. We conclude that the formula (5) is adequate for our present purposes.

5. Concluding remarks

The current study has made use of microstructural observations and macroscopic measurements of modulus in order to develop a micromechanical model for the stiffness of porcine adipose tissue. The models suggest that adipose tissue behaves as a closed cell foam such that the effective modulus is controlled by the stiffness of the reinforced basement membrane. The effect of volumetric constraint by the liquid is to increase slightly the effective stiffness of the reinforced basement membrane. The septa fibres play only a secondary role in dictating the macroscopic modulus. Thus, Eq. (5) is an adequate description for the modulus of adipose tissue.

The analysis presented above for a fluid-filled closed cell foam is directly relevant to the problem of turgor pressure in plants. Plant tissue comprises liquid-filled cells with cell walls reinforced by cellulose. Under the internal turgor pressure the cell walls become pre-stretched and the alignment of the cellulose fibres within the walls leads to an increased modulus of the cellulose, and thereby to an increase in macroscopic modulus in accordance with (5). This explanation is consistent with that given previously by Warner et al. (2000).

Acknowledgements

The authors are grateful for financial support from the EPSRC, from Novo Nordisk A/S, Denmark and are grateful to Dr. Jeremy Skepper at Cambridge University Multi-imaging centre for his support and assistance.

Appendix A. Tissue preparation for microscopy

A.1. Tissue preparation for scanning electron microscopy (SEM)

Samples of fresh porcine adipose tissue from the jowl of a pig were obtained from Dalehead Foods, Linton, Cambs., UK. The tissue was stored in phosphate buffered saline (PBS) for transport (4 h). Tissue sections were prepared at the Multi-Imaging Centre, department of Physiology Development and Neuroscience, University of Cambridge according to the following procedure:

(i) The tissue was fixed in Gluteraldehyde for 2 days. All the tissue was fixed within 6 h of harvesting.
(ii) The tissue was repeatedly washed in de-ionised water.
(iii) Aqueous solutions of 70%, 95% and 100% ethanol were used to dehydrate the tissue. The tissue was soaked for 24 h at each concentration.
(iv) The tissue was then soaked in 50/50 Chloroform and methanol with five changes in 24 h at room temperature.
(v) This was followed by a soak in 50/50 Chloroform and methanol with two changes in 24 h at 53 °C.
(vi) The tissue was placed in 100% Xylene for 1 day at 53 °C to remove the lipid content, the presence of the lipid would otherwise obscure the microscopic images.
(vii) Ethanol followed by de-ionised water was used to rehydrated the tissue.
(viii) The tissue was placed in 7 Molar HCl overnight, then washed: HCl breaks down the phospholipid membranes.
(ix) The tissue was placed in an aqueous solution of 1% osmium tetroxide. Osmium tetroxide further fixes the proteins and molecules with double bonds and increases the electron density, improving the quality of the SEM image.
(x) Excess osmium tetroxide was washed off with de-ionised water.
(xi) Finally the tissue was critical point dried, and coated with a thin layer of gold.

A.2. Tissue preparation for confocal microscopy

Samples of fresh porcine adipose tissue from the jowl of a pig were procured as in Appendix A.1 and were subjected to the following treatment:

(i) The tissue was fixed in Bouin's fixative for two days. All the tissue was fixed within 6 h of harvesting.
(ii) The tissue was subjected to the steps (ii)–(viii) of Appendix A.1.
(iii) The collagen content of the tissue was stained with 1% picro sirus red (Junqueira et al., 1979).

A.3. Histological tissue preparation

As above, fresh porcine adipose tissue from the jowl of a pig was stored in PBS for transport (4 h). The tissue sections were processed for light microscopy in a Histokinette (Leica, Germany) and then embedded with random orientation in paraffin and sliced into 4 μm sections. The sections were stained with hematoxylin, counterstained with eosin, and then mounted on a coverslide with DPX glue (BDH, Poole, UK). The processing was undertaken by the department of Histopathology, University of Cambridge.

References

Abrahamson, D.R., 1986. Recent studies on the structure and pathology of basement membranes. J. Pathol. 149 (4), 257–278.
Angel, A., Sheldon, H., 1965. Adipose cell organelles: isolation, morphology and possible relation to intracellular lipid transport. Ann. NY Acad. Sci. 131 (1), 157–176.
Barnes, H.A. et al., 1993. An Introduction to Rheology. Elsevier.
Benedict, J.V. et al., 1968. Stress–strain characteristics and tensile strength of unembalmed human tendon. J. Biomech. 1 (1).
Bjorntorp, P., Martinsson, A., 1966. The composition of human subcutaneous adipose tissue in relation to its morphology. Acta Med. Scand. 179 (4), 475–481.
Brocca, M. et al., 2001. Microplane model for stiff foams and finite element analysis of sandwich failure by core indentation. Int. J. Solids Struct. 38 (44–45), 8111–8132.
Brockerhoff, H. et al., 1966. Positional distribution of fatty acids in triglycerides of animal depot fats. Biochim. Biophys. Acta 116 (1), 67–72.
Brooks, J.S.J., Perosio, P.M., 1997. Adipose tissue. In: Sternberg, S.S. (Ed.), Histology for Pathologists, second ed. Lippincott-Raven, pp. 167–196.
Budiansky, B., Kimmel, E., 1987. Elastic-moduli of lungs. ASME J. Appl. Mech. 54 (2), 351–358.
Candiello, J. et al., 2007. Biomechanical properties of native basement membranes. FEBS J. 274 (11), 2897–2908.
Codd, S.L. et al., 1994. Tensile stiffness of ovine tracheal wall. J. Appl. Physiol. 76 (6), 2627–2635.
Comley, K., Fleck, N.A., 2009. The high strain rate response of adipose tissue. In: IUTAM Symposium on Mechanical Properties of Cellular Materials, vol. 12, pp. 27–33.

Cormack, D.H., 1987. Ham's Histology, nineth ed. J.B. Lippincott Company.
Crassous, J.J. et al., 2005. Characterization of the viscoelastic behavior of complex fluids using the piezoelastic axial vibrator. J. Rheol. 49 (4), 851–863.
Douglas, W.R., 1972. Pigs and men and research-review of applications and analogies of pig, sus scrofa, in human medical-research. Space Life Sci. 3 (3), 226.
Fung, Y., 1975. Stress, deformation, and atelectasis of the lung. Circ. Res. 37 (4), 481–496.
Geerligs, M. et al., 2008. Linear viscoelastic behavior of subcutaneous adipose tissue. Biorheology 45 (6), 677–688.
Gefen, A., Haberman, E., 2007. Viscoelastic properties of ovine adipose tissue covering the gluteus muscles. ASME J. Biomech. Eng. 129 (6), 924–930.
Georget, D.M.R. et al., 2003. Modelling of carrot tissue as a fluid-filled foam. J. Mat. Sci. 38 (9), 1933–1938.
Gibson, L.J., Ashby, M.F., 1997. Cellular Solids: Structure and Properties, second ed. Cambridge University Press, Cambridge.
Goldberg, B., Rabinovitch, M., 1983. Connective tissue. In: Weiss, L. (Ed.), Histology, Cell and Tissue Biology, fifth ed. Macmillian, pp. 139–177.
Gong, L. et al., 2005. Compressive response of open-cell foams. Part I: Morphology and elastic properties. Int. J. Solids Struct. 42 (5–6), 1355–1379.
Greenwood, M.R.C., Johnson, P.R., 1983. The adipose tissue. In: Weiss, L. (Ed.), Histology, Cell and Tissue Biology, fifth ed. Macmillan, pp. 178–199.
Haake, A. et al., 2001. Structure and function of the skin: overview of the dermis and epidermis. In: Freinkel, R., Woodley, D.T. (Eds.), The Biology of the Skin. The Parthenon Publishing Group.
Haut, R.C., 1983. Age-dependent influence of strain rate on the tensile failure of rat-tail tendon. ASME J. Biomech. Eng. 105, 297–299.
Huber, A.T., Gibson, L.J., 1988. Anisotropy of foams. J. Mat. Sci. 23 (8), 3031–3040.
Jang, W.Y. et al., 2008. On the microstructure of open-cell foams and its effect on elastic properties. Int. J. Solids Struct. 45 (7–8), 1845–1875.
Junqueira, L. et al., 1979. Picrosirius staining plus polarization microscopy, a specific method for collagen detection in tissue sections. Histochem. J. 11 (4), 447–455.
Lodish, H. et al., 2004. Molecular Cell Biology, fifth ed. W.H. Freeman & Co..
Maziak, D.E. et al., 2007. Fourier-transform infrared spectroscopic study of characteristic molecular structure in cancer cells of esophagus: an exploratory study. Cancer Detect. Prev. 31 (3), 244–253.
Mersmann, H.J. et al., 1975. Development of swine adipose tissue: morphology and chemical composition. J. Lipid Res. 16 (4), 269–279.
Miller-Young, J.E. et al., 2002. Material properties of the human calcaneal fat pad in compression: experiment and theory. J. Biomech. 35 (12), 1523–1531.
Myking, A.O., 1988. Studies on the volumetric composition of lymph nodes: problems of efficient sampling and the use of point counting versus digitizer tablets. In: Reith, A., Mayhew, T.M. (Eds.), Stereology and Morphometry in Electron Microscopy: Problems and Solutions. Hemisphere Publishing Corporation, pp. 47–62.
Nakajima, I. et al., 1998. Adipose tissue extracellular matrix: newly organized by adipocytes during differentiation. Differentiation 63 (4), 193–200.
Nightingale, K. et al., 2003. Shear-wave generation using acoustic radiation force: in vivo and ex vivo results. Ultrasound Med. Biol. 29 (12), 1715–1723.
Patel, P.N. et al., 2005. Rheological and recovery properties of poly(ethylene glycol) diacrylate hydrogels and human adipose tissue. J. Biomed. Mat. Res. Part A 73A (3), 313–319.
Rajan, K., 1985. Linear elastic properties of trabecular bone – a cellular solid approach. J. Mat. Sci. Lett. 4 (5), 609–611.
Reith, A., Mayhew, T.M., 1988. Stereology and Morphology in Electron Microscopy. Hemisphere Publishing Corporation.
Sanjeevi, R. et al., 1982. A viscoelastic model for collagen-fibers. J. Biomech. 15 (3), 181–183.
Schoemaker, I. et al., 2006. Elasticity, viscosity, and deformation of orbital fat. Invest. Ophthalmol. Visual Sci. 47 (11), 4819–4826.
Shaw, H.B., 1901. A contribution to the study of the morphology of adipose tissue. J. Anat. Physiol. 36 (Pt 1), 1–13.
Sheldon, H., 1965. Morphology of adipose tissue: a microscopic anatomy of fat. In: Renold, A.E., Cahill, G.F. (Eds.), Handbook of Physiology. Section 5: Adipose Tissue. American Physiological Society, p. 125.
Shergold, O.A., Fleck, N.A., 2004. Mechanisms of deep penetration of soft solids, with application to the injection and wounding of skin. Proc. R. Soc. London, Ser. A 460 (2050), 3037–3058.
Snider, M.D. et al., 2006. Lipid metabolism1: synthesis, storage and utilization of fatty acids and triacyglcerols. In: Devlin, T.M. (Ed.), Textbook of Biochemistry with Clinical Correlations, sixth ed. Willey-Liss, pp. 661–694.
Sullivan, R.M. et al., 2008. A general tetrakaidecahedron model for open-celled foams. Int. J. Solids Struct. 45 (6), 1754–1765.
Urmacher, C.D., 1997. Normal skin. In: Sternberg, S.S. (Ed.), Histology for Pathologists, second ed. Lippincott-Raven, pp. 25–45.
Vawter, D.L. et al., 1979. Constitutive equation of lung-tissue elasticity. J. Biomech. Eng. – Trans. ASME 101 (1), 38–45.
Warner, M. et al., 2000. The elasticity and failure of fluid-filled cellular solids: theory and experiment. Proc. Nat. Acad. Sci. USA 97 (4), 1370–1375.